Multivariate regression trees as an 'explainable machine learning' approach to exploring relationships between hydroclimatic characteristics and agricultural and hydrological drought severity. Case of study Cesar River basin.

Ana Paez-Trujilo[1,2,3], Jeffer Cañon[3], Beatriz Hernandez[3], Gerald Corzo[1], Dimitri Solomatine[1,2,4]

[1]IHE Delft Institute for Water Education, P.O. Box 3015, 2601 DA Delft, the Netherlands
[2]Delft University of Technology, Water Resources Section, P.O. Box 5048, 2600 GA Delft, the Netherlands
[3]Fundacion Natura Colombia, P.O. 111311, Carrera 21 No. 39–43 Bogotá D.C., Colombia
[4]RAS Water Problems Institute, 119333, Moscow, Russia

Correspondence to: Ana M. Paez-Trujilo[1] (A.M.PaezTrujillo@tudelft.nl)

Abstract

The typical drivers of drought events are lower precipitation and/or higher than normal evaporation. The region's characteristics may enhance or alleviate the severity of these events. Evaluating the multiple factors that influence droughts is complex and requires innovative approaches. To address this complexity, we apply hydrological modelling and a machine learning tool to assess the relationship between hydroclimatic characteristics and the severity of agricultural and hydrological droughts. The Soil Water Assessment Tool is used for hydrological modelling. Model outputs, soil moisture and streamflow are used to calculate the drought indices Soil Moisture Deficit Index and the Standardized Stream Flow Index. Drought indices are utilised to identify the agricultural and hydrological drought events during the period of analysis and describe their severity. Then, the Multivariate regression tree technique is applied to assess the relationship between hydroclimatic characteristics (represented by different simulated hydroclimatic parameters) and the severity of agricultural and hydrological droughts.

Our research indicates that multiple parameters influence the severity of agricultural and hydrological droughts in the Cesar River Basin. The upper part of the river valley is very susceptible to agricultural and hydrological drought. Precipitation shortfalls and high potential evapotranspiration drive severe agricultural drought. Limited precipitation influences severe hydrological drought. In the middle part of the river, inadequate rainfall partitioning and an unbalanced water cycle that favours water loss through percolation and evapotranspiration cause severe agricultural and hydrological drought conditions. Finally, droughts are moderate in the basin's southern part (Zapatosa marsh and the Serrania del Perijá foothills). Moderate exposure to agricultural and hydrological droughts is related to the capacity of the subbasins to retain water, which lowers evapotranspiration losses and promotes percolation. Results show that the presented methodology, combining hydrologic

modelling and a machine learning tool, provides valuable information about an interplay between the hydroclimatic factors that influence drought severity in the Cesar River basin.

1 Introduction

Projections indicate that drought frequency, severity and duration are expected to increase globally in the twenty-first century (UNDRR, 2021). Upcoming soil moisture drought scenarios predict statically significant, large-scale drying, especially in scenarios with strong radiative forcing in Central America and tropical South America United States Department of Agriculture (Lu et al., 2019). A similar trend is predicted for hydrological drought severity. This is expected to increase by the end of the twenty-first century, with regional hotspots in central and western Europe and South America, where the frequency of hydrological drought may increase by more than 20 % (Prudhomme et al., 2014). The intensification of drought characteristics (in combination with other factors) could force the migration of up to 216 million people by 2050 (The World Bank, 2021), increase wildfire risk and tree mortality, and negatively affect regional air quality, among other ecosystem impacts (Vicente-Serrano et al., 2020).

It is essential that we better understand drought drivers if we are to foster preparedness and resilience to projected drought events. Remarkable progress has been achieved in understanding drought propagation through the hydrological cycle (Van Loon et al., 2012). Drought occurs due to climatic extremes, which may be enhanced or alleviated by region characteristics and anthropogenic influence (Hao et al., 2022; Seneviratne et al., 2012; Tijdeman et al., 2018). Typically, droughts are triggered by atmospheric circulation and weather systems that combine to cause lower precipitation and/or higher than normal evaporation in a region (Destouni & Verrot, 2014; Sheffield & Wood, 2011a). Reduced precipitation leads to a decrease in soil moisture, causing agricultural drought. When soil moisture depletion is high, it is restored in the wet season, thus reducing subsurface flow and groundwater recharge and giving rise to hydrological drought (Iglesias et al., 2018). Regional characteristics such as soil type, elevation, slope, vegetation cover, drainage networks, water bodies and groundwater systems play a relevant role in response to the climate anomalies that affect drought propagation and contribute to different levels of agricultural and hydrological drought (Sheffield & Wood, 2011a; Zhang et al., 2022). Equally important, human interventions in the hydrological cycle (e.g. reservoirs, water diversion, deforestation, over-pumping groundwater, overgrazing, urbanisation) can reduce water supplies, triggering a drought situation or exacerbating a climate-driven drought (Rangecroft et al., 2019; Wang et al., 2021).

Drought planning also uses research progress on drought characterisation. Various methodologies for drought characterisation exist, and using drought indices is widespread (Zargar et al., 2011). Drought indices are computed numerical representations of drought severity (Hao & Singh, 2015; Keyantash & Dracup, 2002). Severity refers to the departure from the normal of an index. Generally, severity is divided into different categories (e.g. moderate, severe, extreme), providing a qualitative

assessment of the drought state in a region during a given period. Drought indices (and their categories) are crucial for tracking or anticipating drought-related damage and impacts (WMO & GWP, 2016).

Despite remarkable progress achieved in understanding the drought-generating process and drought characterisation, there is still a need for studies that assess the complex interplay between the different drivers of droughts and how their combined effect influences drought characteristics (e.g. duration, severity, intensity) (Valiya Veettil & Mishra, 2020). Previous studies focus on the influence of one driver (Margariti et al., 2019; Mastrotheodoros et al., 2020; Shah et al., 2021; Xu et al., 2019), and some of the methodologies applied cannot adequately address the non-linear relationship between climate, basin processes and droughts characteristics (Peña-Gallardo et al., 2019; Saft et al., 2016; Van Loon, 2015).

We have found two studies that employ machine learning to analyse the non-linear relationship between climate and basin processes and droughts (Konapala & Mishra, 2020; Valiya Veettil & Mishra, 2020). Valiya Veettil et al. (2020) used a classification and regression tree (CART) to identify the variables influencing drought duration. Since CART allows one output variable (drought duration), the authors applied the technique three times to evaluate the variables influencing short-term, medium-term and long-term drought events. Meanwhile, Konapala et al. (2020) used a random forest (RF) algorithm to identify the climate and basin parameters influencing the characteristics (duration, frequency and intensity) of three different drought regimes (long duration and mild intensity, moderate duration and intensity, short duration and high intensity). As the core of RF is a decision tree that allows one output variable (in this case, each characteristic of each drought regime), the authors repeated the procedure for each drought regime and characteristic. Both studies focused on drivers of hydrological drought.

Mentioned research shows the potential of machine learning techniques for drought-related analysis; nevertheless, there is still a need for testing a technique capable of simultaneously assessing the influence of different drought drivers on the individual categories of drought severity. Commonly used in the field of ecology to relate independent environmental conditions to populations of multiple species, Multivariate Regression Tree (MVRT) arises as a suitable technique for this purpose. MVRT is a supervised clustering technique that links explanatory variables to multiple response variables while maintaining the individual characteristics of the responses. Significantly, the technique does not assume a linear relationship between explanatory and response variables. Furthermore, it allows for the so-called “interpretable machine learning” algorithms that make decisions and predictions understandable to humans (Molnar, 2022). MVRT interpretably is a relevant attribute for drought researchers and planners since the method allows them to identify the parameters influencing severe (or mild) drought conditions.

To understand the relationship between the drivers of droughts and the individual categories of agricultural and hydrological droughts severity, this study employs a methodology that consists of three steps. The first is hydrological modelling. We used Soil Water Assessment Tool (SWAT) to simulate the hydroclimatic parameters required for analysing droughts and applying

the MVRT approach. The Second is the analysis of droughts. SWAT outputs, soil moisture and streamflow are used to calculate the drought indices Soil Moisture Deficit Index (SMDI) and the Standardized Stream Flow Index (SSI). Drought indices are utilised to identify the agricultural and hydrological drought events during the period of analysis and describe their severity. Finally, the MVRT approach is applied to assess the relationship between hydroclimatic characteristics (represented by the simulated parameters at each subbasin, see Table 2) and droughts severity categories (represented by the observed number of months for each drought severity category at each subbasin, see Table 3). The analyses for agricultural and hydrological droughts were conducted separately; thus, two MVRTs were obtained. A concrete application of this methodology is developed in the Cesar River basin (Colombia, South America).

2 Study location and methods

2.1 Case study

Figure 1 presents the Cesar River basin's location, topography and land use. The basin is located between 72º53'W 74º04'W and 10º52'00'N 7º41'00''N latitude (Colombia). It extends for an area of 22,312 km^2. The basin's topography is defined in three distinct climatic regions (Universidad del Atlantico, 2014). In the north is La Sierra Nevada de Santa Marta. This sector is characterised by steeply sloped mountains reaching up to 5,700 meters above sea level (masl). The temperature ranges from 3°C to 6°C, and the mean annual precipitation is 1,000 mm. In the east is La Serranía del Perijá. This mountainous area is an extension of the eastern branch of the Andes range. In this sector, the altitude ranges from 1,000 to 2,000 masl. The average temperature is 24°C, and the average annual precipitation varies from 1,000 mm to 2,000 mm. Lastly, the valley of the Cesar River and the Zapatosa marsh are in the west and south of the basin, respectively. The valley is characterised by flat topography and a complex system of marshes formed by the Cesar River floodplains and its confluence with the Magdalena River. The average temperature is 28°C, and the mean annual precipitation is 1,500 mm. At the basin, the annual rainfall pattern presents a dry season from December to April, followed by a rainy season from April to May. In the intermediate period from June to July, precipitation decreases. The main rainfall events occur between August and November.

The predominant land use is pasture, followed by agriculture (Universidad del Atlantico, 2014). The primary land use in La Sierra Nevada foothills is pastures for cattle farming. In La Serranía del Perijá, the high-altitude areas are covered by forests in very good condition; at the lower altitudes, the principal land use is agriculture, particularly subsistence crops. The Cesar River valley's soils are rich in nutrients, providing favourable conditions for agriculture. The riverbanks are covered by forests with low tree density.

The Zapatosa marsh is recognised as one of the most important wetlands in the country, and considering the relevance of this ecosystem, it was declared a Ramsar site in 2018. Nevertheless, the region is threatened by high water demand of monocrops and overexploitation of its forest resources. In addition, climate change projections indicate that the basin's temperature may

increase by 2.7°C, and precipitation may reduce by 10 % by 2070 (Universidad del Magdalena et al., 2017). Accordingly, multiple initiatives are oriented to improve water management and create resilience to hydroclimatic extremes (Ministerio de Ambiente y Desarrollo Sostenible (Colombia), 2015).

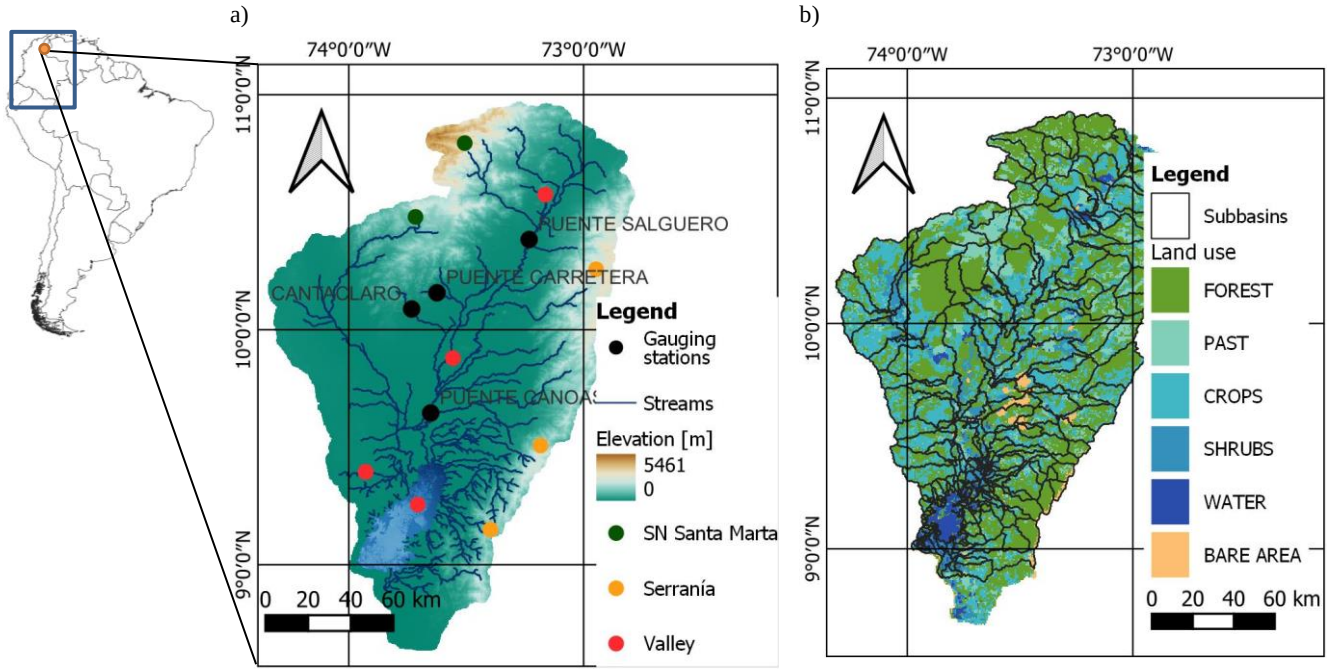

Figure 1 Cesar River basin: a) topography and b) land use.

2.2 Methods

Figure 2 illustrates the three steps methodology applied in this study. Section 2.2.1 describes the hydrological modelling, and 2.2.2 the drought analysis. Section 2.2.3 presents the application of the MVRT technique.

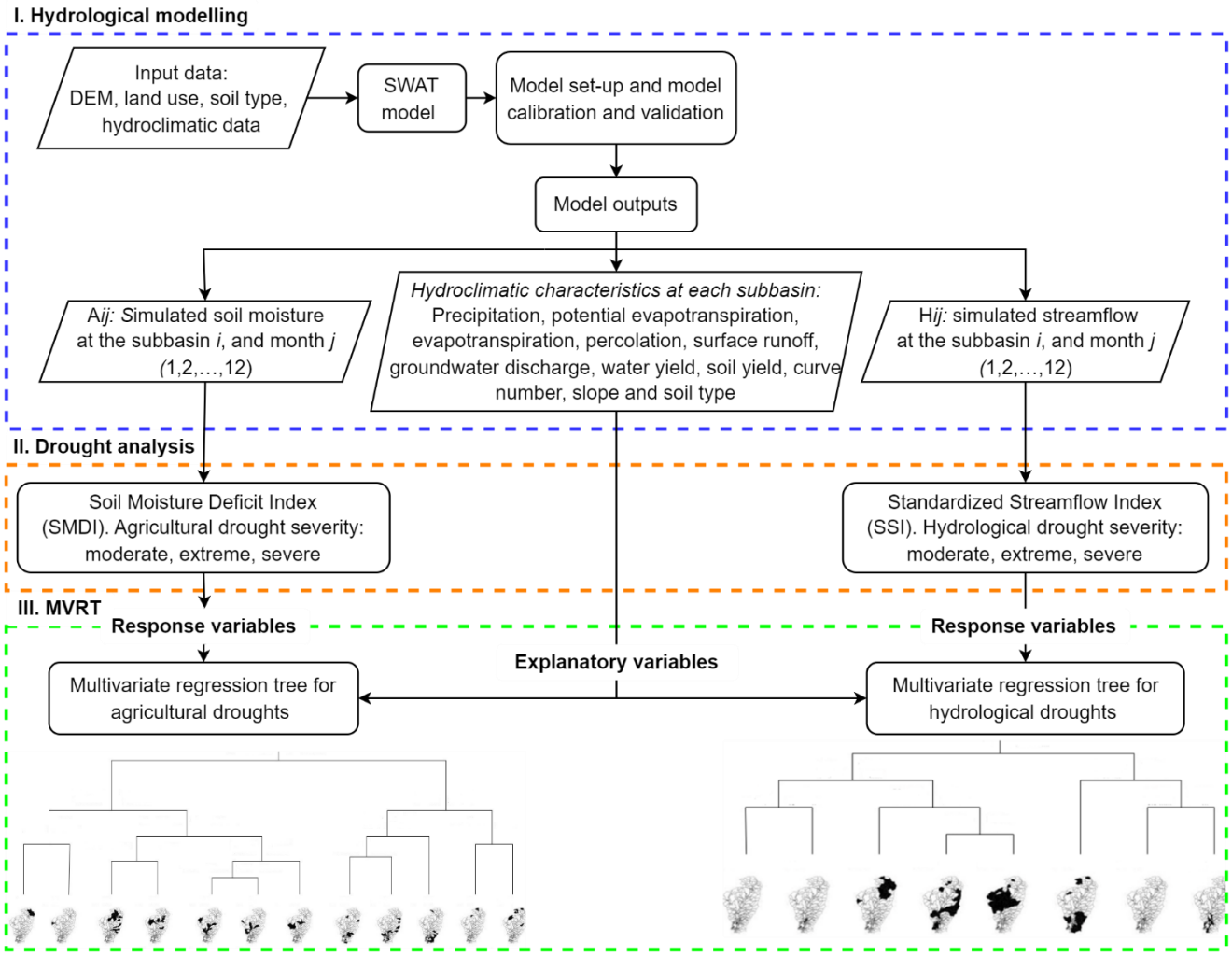

Figure 2 Flow chart of the methodology.

2.2.1 Hydrological modelling

A SWAT model with an ArcSWAT extension was used to develop the hydrological model of the Cesar River. SWAT is a continuous-time, semi-distributed, process-based river watershed-scale model developed by The Agricultural Research Service of the United States Department of Agriculture (ARS-USDA). The model is designed to simulate the quality and quantity of surface and groundwater and predict the environmental impacts of land management and climate change (Neitsch et al., 2011). In SWAT, the basin area up to the outlet point is divided into several subbasins. Each subbasin is further split into multiple Hydrological Response Units (HRU), which are areas within the subbasin with common combinations of land cover, soil type and slope (Arnold et al., 2012).

Model setup

The model was built for the period from 1987 to 2018. The Cesar River basin was divided into 313 subbasins with a median area of 50 km^2. Four slope classes were set for the HRUs generation: flat (0–2%), gentle (2–10%), steep (10–35%) and considerably steep (>36%) (GEF et al., 2020, 2021). The following methods were used to model the principal hydrological processes: the soil conservation services-curve number (SCS-CN) was used to simulate surface runoff; potential evapotranspiration was estimated using the Hargreaves method; and water was routed through the channel network using the variable storage routing method. The details and sources of the SWAT model input data are presented in Table 1.

Table 1. SWAT model input data

Data type	Details	Source
Digital elevation model	25 × 25 m	Dataset ALOS PALSAR L1.0, Cartography 1:25000 Geographic Institute Agustín Codazzi (IGAC), Colombia
Soil map	300 × 300 m	Soil profiles Project GEF Magdalena–Cauca VIVE, GEF, BID, Fundación Natura, Colombia
Land use map	25 × 25 m	Land use map Geographic Institute Agustin Codazzi (IGAC), Colombia
Rainfall and temperature daily data	Period 1985–2018 (34 years)	Institute of Hydrology, Meteorology and Environmental Studies (IDEAM), Colombia
Discharge monthly data (Gauging stations Figure 1)	Period 1985–2018 (34 years)	Institute of Hydrology, Meteorology and Environmental Studies (IDEAM), Colombia

Model calibration and validation

We used the SWAT-CUP software package with Sequential Uncertainty Fitting version 2 (SUFI-2) to evaluate the model's performance in simulating streamflow for automatic model calibration and validation. With SUFI-2, parameter sensitivities are determined by applying a multiple regression approach, which regresses the parameters sampled via a Latin hypercube technique against the objective function values (Abbaspour et al., 2018).

Based on expert judgment and the available literature (Arnold et al., 2012; Transactions of the ASABE (American Society of Agricultural and Biological Engineers), 2018), the following SWAT parameters were used in the calibration and validation process: baseflow alpha factor (ALPHA_BF), effective hydraulic conductivity in main channel alluvium (CH_K), Manning's value for the main channel (CH_N2), SCS runoff curve number for moisture condition II (CN2), soil evaporation compensation factor (ESCO), groundwater delay (GW_DELAY), threshold depth of water in the shallow aquifer required for return flow to occur (GWQMN), deep aquifer percolation fraction (RCHRG_DP), threshold depth of water in the shallow aquifer for percolation to the deep aquifer to occur (REVAPMN) and available water capacity of the soil layer (SOL_AWC).

The model was calibrated from 1985 to 2002 and validated from 2003 to 2018 using the streamflow series from four stream gauges (Figure 1). The first two years were used as a warming-up period in both cases. Thus, performance indicators were calculated for 1987 to 2002 (calibration) and 2005 to 2018 (validation). The model was evaluated using the Nash-Sutcliffe Efficiency (NSE) and percent bias (PBIAS), represented by Eq. 1 and Eq. 2, respectively:

$$NSE = 1 - \frac{\sum_{i=1}^{N}(O_i - P_i)^2}{\sum_{i=1}^{N}(O_i - \bar{O})^2} \quad (1)$$

$$PBIAS = \frac{\sum_{i=1}^{N}(O_i - P_i) \times 100}{\sum_{i=1}^{N} O_i} \quad (2)$$

where O_i is the observed data, P_i the predicted data, $\bar{O}$ the mean of the observed data and N the number of observations during the simulation period.

The NSE represents a dimensionless indicator ranging from -∞ to 1, with 1 representing a perfect match between the observed and simulated values (Moriasi et al., 2007). The PBIAS measures the average tendency of the simulated values to be larger or smaller than the observed values. A low PBIAS magnitude indicates accurate model simulation (Moriasi et al., 2007).

2.2.2 Agricultural and hydrological drought analysis

The present study used the soil moisture deficit index (SMDI) to analyse agricultural droughts (Narasimhan & Srinivasan, 2005). The input parameter used to calculate the SMDI was the simulated soil water in the soil profile at each subbasin. SWAT calculates the soil water content of the entire soil profile. According to the soil profiles used to elaborate the soil map, three soil layers were identified in the Cesar River basin. The soil layers' thickness (vertical distance from the surface) varies. The first layer reaches up to 350 mm, the second 1000 mm, and the third 1500 mm.

The computation procedure to determine the soil moisture deficit used the long-term soil moisture characteristics and the soil moisture conditions during the drought period. The indicator was scaled between -4 to 4 to allow the spatial comparison of the drought index, regardless of climatic characteristics (Narasimhan & Srinivasan, 2005). Negative values of SMDI indicate dry periods, while positive values indicate wet periods (compared to the region's normal conditions). Per the SMDI, agricultural drought severity was divided into three categories: moderate drought (SMDI -2.0 to -2.99), severe drought (SMDI -3.0 to -3.99) and extreme drought (SMDI -4 or less). The following procedure was applied to compute the SMDI at each subbasin:

$$SD_{ij} = \frac{SW_{ij} - MSW_j}{MSW_j - minSW_j} \times 100, \qquad if\ SW_{ij} \leq MSW_j \quad (3)$$

$$SD_{ij} = \frac{SW_{ij} - MSW_j}{maxSW_j - MSW_j} \times 100, \qquad if\ SW_{ij} > MSW_j \quad (4)$$

where SD_j is the soil moisture deficit (%), SW_j is the monthly soil water available in the soil profile (mm) and MSW_j, $maxSW_j$ and $minSW_j$ are long-term median, maximum and minimum soil water available in the soil profile (mm), respectively, ($i = 1987 - 2018\ and\ j = 1 - 12$).

The $SMDI_j$ of any given month was calculated using Eq. 5:

$$SMDI_j = 0.5 \times SMDI_{j-1} + \frac{SD_j}{50} \quad (5)$$

where $SMDI_{j-1}$ is the SMDI from the previous month.

SMDI was not calculated for the subbasins that correspond to the Zapatosa marsh. In these subbasins the predominant land cover is water. See Figure 5.

We used a standardised streamflow index (SSI) to represent hydrological droughts. The indicator was introduced by Modarres (2007) and further investigated by Vicente-Serrano et al. (2011). The index is statically analogous to the commonly used standardised precipitation index (SPI) introduced by Mckee et al. (1993). SSI values mainly range from -2.0 (extremely dry) to 2.0 (extremely wet), and hydrological drought severity is divided into three categories: moderate drought (SSI -1.0 to -1.49), severe drought (SSI -1.5 to -1.99) and extreme drought (SSI -2.0 or less). The procedure to calculate SSI consists of converting streamflow values to standardised anomalies (i.e. z-scores). To this aim, the monthly simulated streamflow at each subbasin in the analysis period (1987 to 2018) was fitted to the gamma probability distribution function.

SMDI and SSI were calculated monthly using the simulated soil water and streamflow values at each subbasin. The drought events during the period of analysis were then identified. A drought (agricultural or hydrological) event was assumed to occur in the basin when a number of subbasins (covering at least 30 % of the basin's total area) were in a moderate drought state for at least two consecutive time steps (i.e. in this study month). According to the spatial and temporal thresholds, a drought event began when both conditions were met and continued until one of them failed to be met. We set a minimum spatial extension threshold because droughts typically extend regionally (Sheffield & Wood, 2011b). By setting the temporal threshold, we avoided identifying periods of water shortage or scarcity as drought events.

2.2.3 Multivariate regression tree approach for evaluating the relationships between hydroclimatic characteristics and droughts severity

MVRT is an extension of a regression tree (Breiman, 2001), but it differs in that it allows for multiple outputs (see De'ath, 2002). It recursively splits a quantitative response variable (predictand, output) controlled by a set of numerical or categorical explanatory variables (predictors, input). The technique approach yields a set of non-linear models, each a piece-wise linear

regression model (of zero order). An MVRT result is a tree whose terminal groups (leaves) of instances (input-output vectors) comprise subsets of samples selected to minimise the within-group sums of squares. Each successive split is given by a threshold value of the explanatory variables (Borcard et al., 2018). MVRT is applied to dataset exploration, description and prediction (De'ath, 2002). In this study, the explanatory variables are the hydroclimatic parameters at each subbasin, represented by the average value of each parameter during the analysis period (1987 to 2018). The response variables are the number of months observed at each drought severity category (the drought indices give categories). The analyses for agricultural and hydrological droughts were conducted separately; thus, two MVRTs were obtained.

Four technique attributes are relevant to this study. First, MVRT can capture the non-linear interactions between the parameters influencing droughts and their severity. Second, the technique can handle numerical and categorical hydroclimatic parameters influencing drought severity (explanatory variables). Third, MVRT's capability to handle multiple outputs allowed us to evaluate the influence of the hydroclimatic parameters on moderate, severe and extreme drought conditions simultaneously (response variables). The drought indicators give these three categories to represent the drought severity. Simultaneous analysis of different drought categories provides a comprehensive understanding of the drought-generating process and the factors influencing severe (or mild) drought conditions. Fourth, MVRT results can be easily visualised and interpreted. The resulting tree structure provides a clear representation of the relationship between the drivers of droughts and the severity of agricultural and hydrological droughts.

To compute the MVRT, we used R software; namely the package mvpart. Before the analysis, the sets of explanatory and response variables were transformed to compare the descriptors measured in different units and to modify the variables' weights. The matrix of explanatory variables was standardised to a mean of zero and a standard deviation of one. The matrix of response variables was standardised by the column maximum, then again by the row total (Wisconsin double standardisation).

Datasets

Set of explanatory variables

To select the set of explanatory variables, we used the outcomes of previous studies on governing drivers of droughts (Sheffield & Wood, 2011a; Zhang et al., 2022). Table 2 describes the eleven parameters selected as the potential drivers of droughts. The used values correspond to the parameters' average in the analysis period (1987 to 2018). The averages were computed using the SWAT model outputs at each subbasin. We used the dominant category at each subbasin for the curve number, the slope, and the soil type (categorical variables).

Table 2. Explanatory variables used in MVRT

Hydroclimatic parameter	Abbreviation	Unit	Definition
Precipitation	PRECP	mm	Average precipitation at each subbasin
Potential evapotranspiration	PET	mm	Average potential evapotranspiration at each subbasin
Evapotranspiration	ET	mm	Average actual evapotranspiration at each subbasin
Percolation	PERC	mm	Average percolation past the root zone
Surface runoff	SURFQ	mm	Average surface contribution to the streamflow at each subbasin
Groundwater	GRWQ	mm	Average groundwater contribution to the streamflow at each subbasin
Water yield	WYLD	mm	Average amount of water that leaves the subbasin and contributes to the streamflow at each subbasin
Sediment yield	SYLD	metric tons/ha	Average sediment from the subbasin transported into the reach
Curve number	CN	–	Dominant curve number at each subbasin
Slope	SLP	–	Dominant slope at each subbasin
Hydrologic soil group	STY	–	Dominant hydrologic soil group (A, B, C, and D) at each subbasin. The U.S. Department of Agriculture (USDA) classify soils in four hydrologic groups based on the soil's infiltration characteristics. Properties of each soil type can be found in USDA (2007)

Set of response variables

We used the drought analysis outcomes to define the response variables (Table 3). Following the methodology presented in 2.3, we identified the agricultural and hydrological drought events during the analysed period. After identifying the drought events, we counted the months for each drought severity category at each subbasin. The observed months for each one of the three drought categories were used as response variables. The analyses for agricultural and hydrological droughts were conducted separately; thus, two sets of response variables were obtained.

Table 3. Response variables used in MVRT

Drought category	Abbreviation	Unit	Definition
Moderate agricultural/hydrological drought	MOD	month	Number of months in the moderate agricultural drought category during the drought events identified in the simulation period at each subbasin
Severe agricultural/hydrological drought	SEV	month	Number of months in the severe agricultural drought category during the drought events identified in the simulation period at each subbasin
Extreme agricultural/hydrological drought	EXT	month	Number of months in the extreme agricultural drought category during the drought events identified in the simulation period at each subbasin

Building the MVRT

Building the MVRT consisted of two processes: (1) the constrained partitioning of the data, and (2) the cross-validation of the results. The mvpart package run both processes in parallel. The two procedures are briefly explained below, and a more detailed description can be found in Borcard et al. (2018).

Constrained partitioning of the data

The data partitioning consisted of three steps. First, for each explanatory variable were generated all possible partitions of the sites (subbasins) into two groups. Second, for each partition, it was calculated the resulting sum of within-group sums of squared distances to the group means for the response data (within-group SS, equivalent to standard deviation). Lastly, the partition into two groups to minimise the within-group SS and the threshold value/level of the explanatory variable was retained. These steps were repeated within the two previously established subgroups until all the objects formed their own groups. For each tree that was computed, the relative error was calculated as the sum of the within-group SS of all leaves divided by the overall SS of the data. This procedure for MVRT is equivalent to the one originally proposed by Breiman (2001) for his regression tree technique.

Cross-validation of the partitions and tree pruning

A cross–validation procedure was used to prune the tree and identify the optimal tree size (Kuhn & Johnson, 2013; Legendre & Legendre, 2012). The cross-validation procedure was performed automatically using mvpart. Per this procedure, the data was randomly divided into roughly equal-sized test groups. Each test group was held out in turn while the tree was fitted using the remaining groups. The distances between the centroids of the tree leaves and each object of the test group were then calculated. Finally, the objects of the test group were allocated to the closest leaf of the constructed tree. An overall relative error statistic (relative cross-validation error, CVRE) was calculated for each group using all *n* objects, per Eq. 6:

$$CVRE_{(k)} = \frac{\sum_{i=1}^{n}\sum_{j=1}^{p}\left(y_{ij(k)} - \hat{y}_{j(k)}\right)^2}{\sum_{i=1}^{n}\sum_{j=1}^{p}\left(y_{ij} - \bar{y}_j\right)^2} \qquad 6$$

where $y_{ij(k)}$ is the value of variable j for object i belonging to test group k, $\hat{y}_{j(k)}$ is the value of that same variable at the centroid of the leaf closest to object i, and the denominator is the overall sum of the Y data squares.

This cross-validation process was repeated several times for consecutive and independent divisions of the data into test groups. For each group, the mean and standard deviation of all CVRE were computed. The CVRE varied from 0 for perfect predictors to close to 1 for poor predictors (for large errors, CVRE may reach $+\infty$). Among the mvpart function arguments, we used ten cross-validation groups (function argument, xval = 10) and 100 iterations (function argument xmult = 100). The tree was selected using interactive cross-validation (function argument xv = 'pick').

To choose the size of the tree that retained the most descriptive partition, we used the approach suggested by De'ath (2002). According to the author a tree with the smallest CVRE offers the best combination of explanatory power and interpretability. Once the tree was built, the proportion of explained variance (EV) was calculated as $1 - RE_{tree}$ (tree relative error) (Cannon, 2012).

3 Results

3.1 SWAT model calibration and validation

Table 4 summarises the calibration and validation performance indicators for the SWAT model at each gauging station. The calibration and validation models simulated monthly stream flows with NSE values equal to or greater than 0.50 and relatively low PBIAS values (GEF et al., 2020, 2021). According to the performance ratings for calibrating and validating hydrological models, NSE and PBIAS values indicated that the model was appropriate for simulating streamflow (Moriasi et al., 2007). Figure 3 presents the model hydrographs at each gauging station for the calibration and validation periods. The locations of the stations can be found in Figure 1.

Table 4. SWAT model performance simulating streamflow

Gauging station	Calibration		Validation	
	NSE	PBIAS [%]	NSE	PBIAS [%]
Puente Salguero	0.61	4.28	0.52	-8.3
Puente Carretera	0.50	-5.34	0.52	7.6
Cantaclaro	0.58	-11.30	0.50	-11.7
Puente Canoas	0.70	-1.34	0.57	10.64

Considering the study focus is on droughts, the model performance simulating low flows was analysed separately. Performance indicators were calculated for the dry season, which lasts from December to March. The intermediate period of precipitation decrease from June to July was also included in this analysis. Table 5 summarises the calibration and validation performance indicators in the dry season. According to the rating guidelines, the model performance simulating low flows is satisfactory (Transactions of the ASABE (American Society of Agricultural and Biological Engineers), 2018).

Table 5. SWAT model performance simulating low flows.

Gauging station	Calibration		Validation	
	NSE	PBIAS [%]	NSE	PBIAS [%]
Puente Salguero	0.65	-19.4	0.53	-21.3
Puente Carretera	0.67	-15.3	0.53	17.2
Cantaclaro	0.67	-3.6	0.58	16.3
Puente Canoas	0.55	-15.7	0.60	-13.5

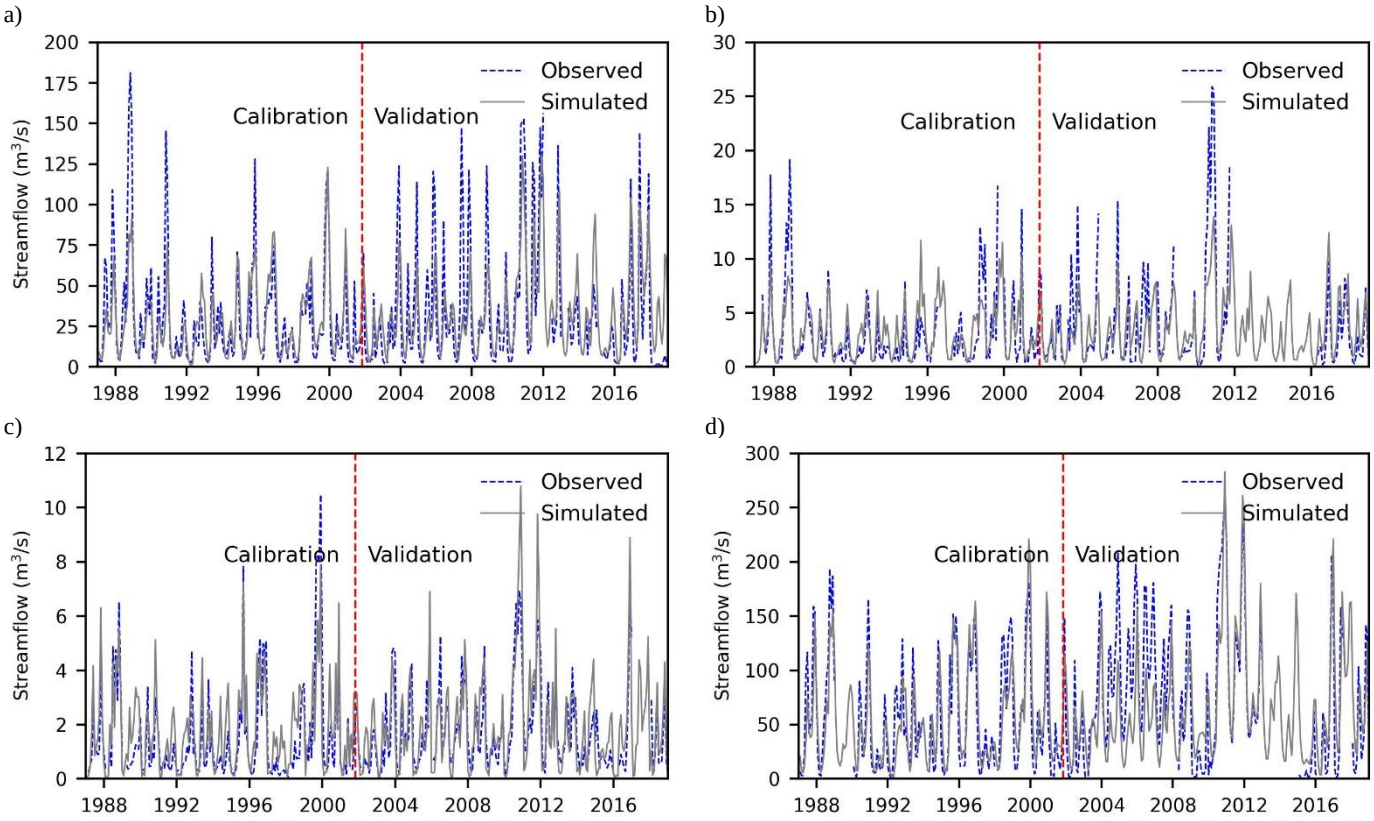

Figure 3 Monthly calibration and validation for streamflow at: a) Puente Salguero, b) Puente Carretera, c) Cantaclaro and d) Puente Canoas.

3.2 Hydroclimatic drivers of droughts

Figure 4 *a* to *h* presents the average value of the numerical hydroclimatic drivers of droughts at each subbasin. The average was calculated using the hydrological model's outputs during the simulation period (1987 to 2018). Figure 4 *i* to *k* presents the categorical drivers: the curve number, slope and soil type. The dominant category at each subbasin is shown in Figure 4 *i* to *k*. The dataset of explanatory variables was created from the values presented in Figure 4.

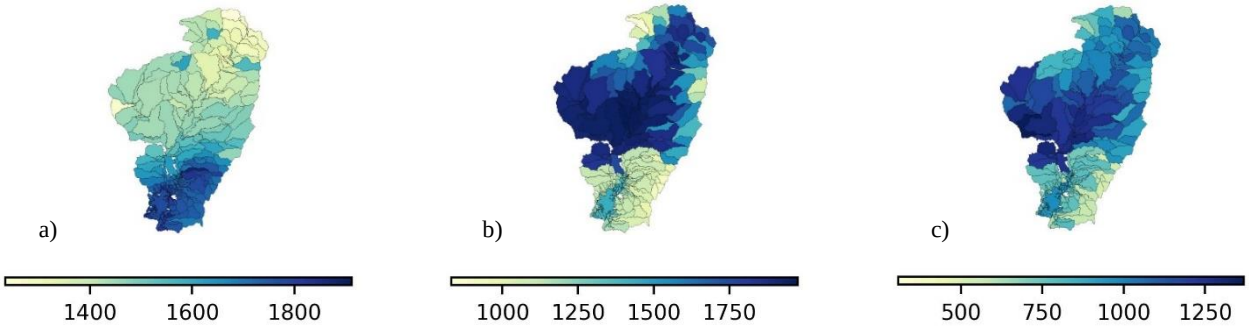

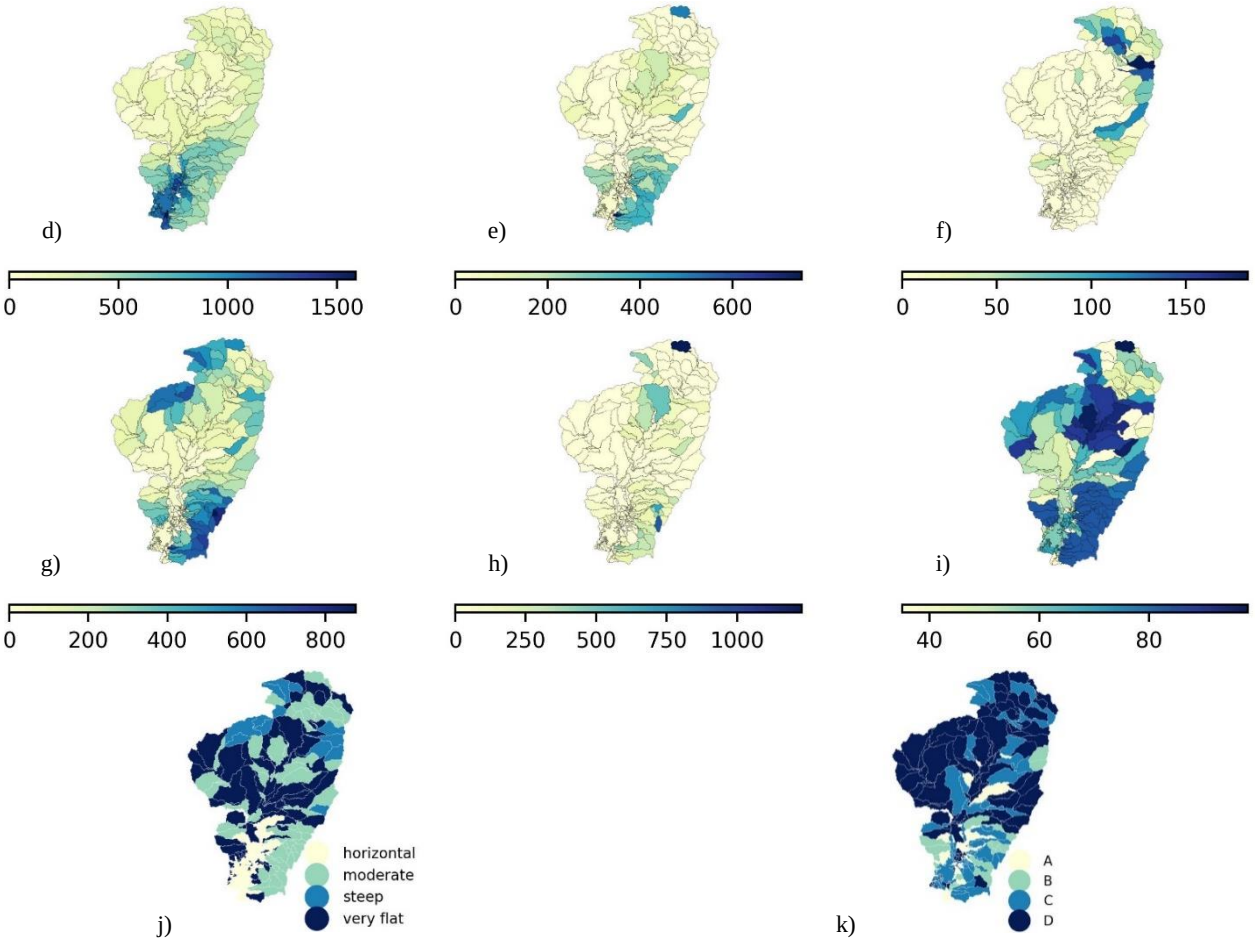

Figure 4 Average value of hydroclimatic parameters during the simulation period at each subbasin: a) precipitation in mm, b) potential evapotranspiration in mm, c) actual evapotranspiration in mm, d) percolation in mm, e) surface runoff in mm, f) groundwater contribution to streamflow in mm, g) water yield in mm, h) sediment yield in metric tons/ha, i) curve number, j) slope and k) soil type.

3.3 Drought events during the simulation period and their duration

Following the methodology described in 2.3, we identified drought events in the analysis period. Table 6 shows the dates and durations of these events. The identified drought events in the simulation period were in good agreement with the chronology of drought events in Colombia described at the National Study of Water (Instituto de Hidrología, 2019).

Table 6. Agricultural and hydrological droughts during the period of analysis

Event	Agricultural droughts		Hydrological droughts	
	Date	**Duration [months]**	**Date**	**Duration [months]**
I	May 1991 – Jun 1992	13	Apr 1991 – May 1992	14
II	Jun 1997 – April 1998	11	Apr 1997 – Feb 1998	11
III	Jun 2001 – Aug 2001	3	May 2001 – Jun 2001	2
IV	Oct 2009 – Jan 2010	4	Sep 2009 – Nov 2009	3
V	Jun 2014 – Aug 2014	3	Jun 2014 – Jul 2014	2
VI	May 2015 – Jul 2016	15	Apr 2015 – Apr 2016	13

After identifying the agricultural and hydrological drought events, it was possible to count the number of months for each drought category in each subbasin. Figure 5 presents the number of months for each agricultural drought category, and Figure 6 presents the number of months for each hydrological drought category. The results presented in Figures 5 and 6 are the response variables for the MVRT technique.

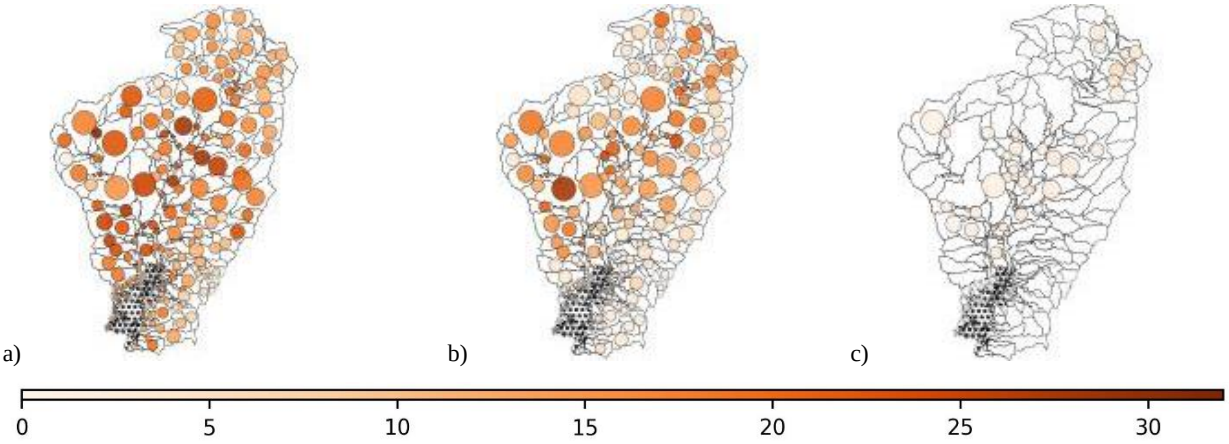

Figure 5 Months counted in each agricultural droughts category: a) moderate, b) severe and c) extreme. SMDI was not calculated in the wetland subbasins (i.e. hatched area).

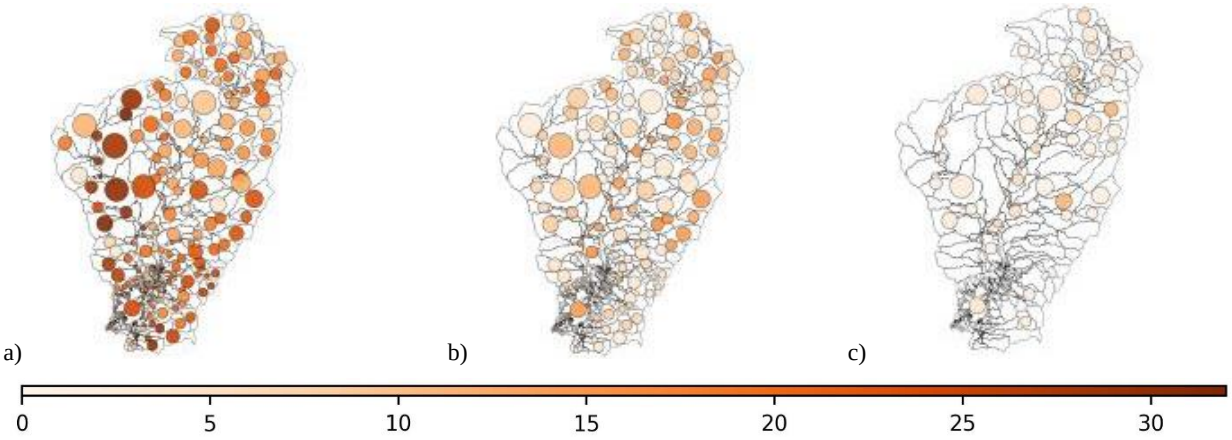

Figure 6 Months counted in the hydrological droughts category: a) moderate, b) severe and c) extreme.

3.4 Multivariate regression tree

In this section, we describe the results of the MVRT technique applied to identify the governing drivers of agricultural and hydrological drought severity and the critical thresholds of these drivers.

3.4.1 Drivers of agricultural drought

Figure 7 presents the tree generated by R software, the number of subbasins clustered at each terminal group (variable "*n*"), and the spatial distribution of these subbasins. The tree consists of five levels of split and twelve leaves. The minimum value of the cross-validation error (CVRE = 0.46) was used to select the tree size. The relative error of the MVRT was 0.19, and the EV was 0.81. Figure 8 presents the tree's numerical output: namely, the number of months for each drought category. The scattering of the outputs in each leaf allows us to identify the subbasins most exposed to agricultural droughts.

The MVRT indicated that evapotranspiration was a strong driver of agricultural droughts; it appeared three times at different tree levels in the splitting rules. The subbasins were split at the first level according to ET (924 mm). At the second level of split, precipitation (1,318 mm) was used for the left branch of the tree and percolation (271 mm) for the right branch. Then, the left branch was recursively split as follows: at the third level, according to potential evapotranspiration (1,888 mm) and evapotranspiration (1,191 mm); at the fourth level, according to evapotranspiration (1,064 mm) and percolation (111 mm); and at the fifth level, according to potential evapotranspiration (1,679 mm) and sediment yield (101 mm). The left branch account for seven out of the tree's twelve leaves. Regarding the right branch, it was divided according to evapotranspiration (729 mm) and the curve number (67) at the third level and according to the water yield (352 mm) at the last level. In the following, we describe agricultural drought MVRT terminal groups.

Leaves *a* and *b*: Leaf *a* clusters seven subbasins in the north part of the basin. In this area, evapotranspiration and potential evapotranspiration were above the basin average, while precipitation was below average. Figure 8a shows that these subbasins experienced the highest number of months in extreme agricultural drought, with a median condition of fifteen months in severe agricultural drought. Leaf *b* clusters two subbasins in the western part of the basin. In this leaf, there are no months in the extreme drought category. The median of months in the moderate and severe agricultural drought categories is ten months, one of the lowest among the terminal groups (Figure 8b).

Leaves *c* and *d* cluster twenty-four and nineteen subbasins, respectively. In leaf *c*, evapotranspiration was above 1,064 mm, a value above the basin average. These subbasins experienced no extreme agricultural droughts, and the median of months in the severe category was below ten, representing the lowest of the left branch of the MVRT (Figure 8b). Leaf *d* shows the highest median of months in the severe drought category (Figure 8b).

Leaves *e*, *f* and *g* cluster twenty-four, six and twelve subbasins, respectively, located in the river valley. In these subbasins, evapotranspiration was higher than 1,991 mm. For leaf *f*, percolation was considerably above the basin average (111 mm), and sediment yield was notably above the median (101 metric tons/ha). Figure 8f, g and h show that the median of months in the moderate drought category was above twenty months; the severe category was above ten months; and the three leaves exhibited months in the extreme drought category.

Leaves *h*, *i* and *j* cluster twenty-six, fifty-two and fifty-six subbasins, respectively. These subbasins are mainly located in the wetland surroundings. Evapotranspiration at terminal groups *i* and *j* was higher than 729 mm. At terminal group *i*, the water yield was higher than the median (352 mm), while at terminal group *j*, it was lower. At leaf *k*, evapotranspiration was lower than 729 mm. The agricultural drought situation in these subbasins was mild. The median of months in the moderate drought category was slightly higher than ten, and the median for months in the severe and extreme categories was the lowest for the area of study (Figure 8h, i, j).

Leaves *k* and *l* cluster two and six subbasins, respectively. In these subbasins, percolation was lower than 271 mm. In leaf *l*, the curve number was lower than sixty-seven, while in leaf *l* it was higher. These subbasins experienced intermediate drought exposure. Figure 8k and l demonstrate that there no months were registered in the extreme drought category.

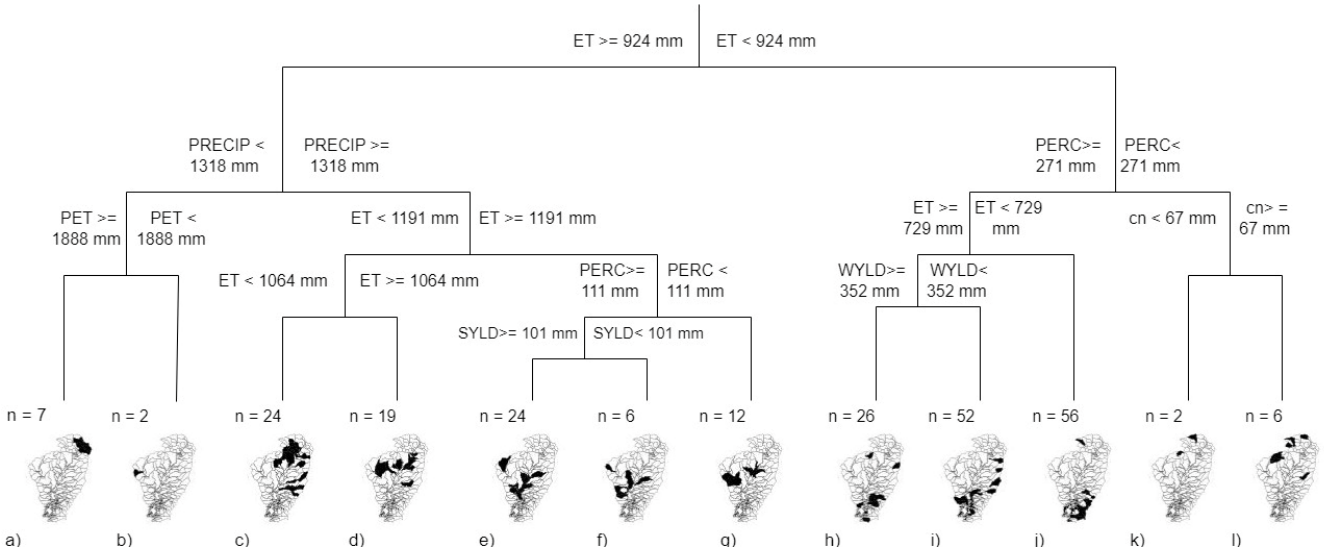

Figure 7 MVRT of hydroclimatic drivers of agricultural droughts at the Cesar River basin, and spatial distribution of the subbasins clustered at each leaf. Tree leaves are named from *a* to *l* and *n* indicates the number of subbasins clustered at each leaf.

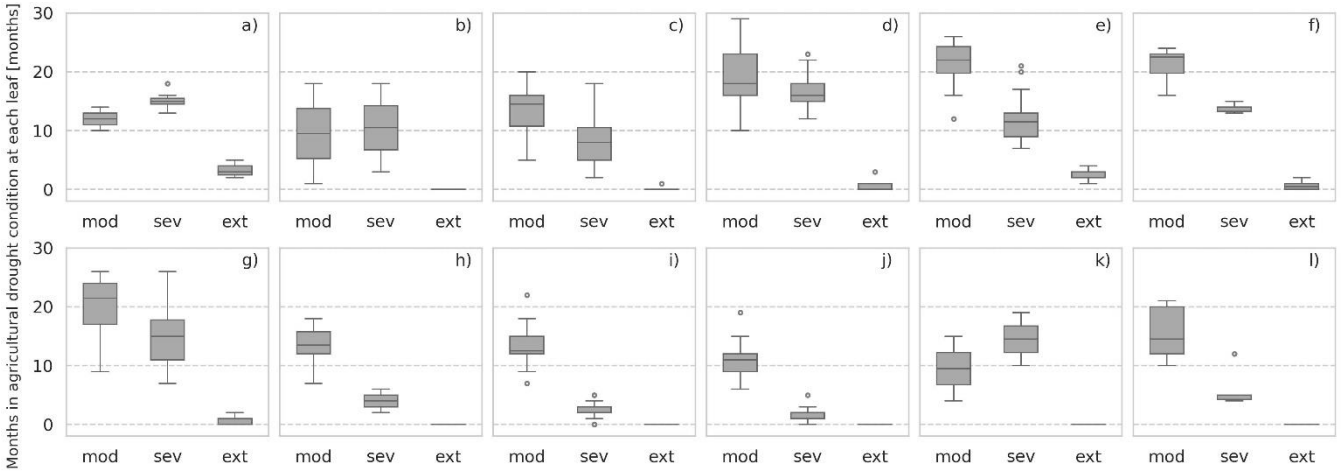

Figure 8 Number of months in agricultural drought categories (moderate, severe, extreme) at each leaf. Tree leaves are named from *a* to *l*.

3.5.2 Drivers of hydrological drought

Figure 9 presents the hydrological drought MVRT, the number of subbasins clustered at each terminal group (variable "*n*") and the spatial distribution of these subbasins. The tree consists of four levels of split and eight leaves. The minimum value of the cross-validation error (CVRE = 0.67) was used to select the tree size. The relative error of the MVRT was 0.52, and the EV was 0.48. Figure 10 presents the tree's numerical output: namely, the number of months for each drought category. This information allowed us to identify the clusters of subbasins most exposed to hydrological droughts.

The MVRT demonstrated that precipitation was a primary driver of hydrological drought; it appeared two times at different levels of split. The subbasins were separated at the first split level according to precipitation (1362 mm). At the second split level, precipitation (1398 mm) was used as the left branch of the tree, and water yield was used as the right branch (29 mm). The left branch was then further divided according to percolation at the third level and according to curve number at the fourth level. Also at the third level, the right branch was split according to evapotranspiration (833 mm) and surface runoff (0.5 mm). The MVRT terminal groups were then examined in detail.

Leaf *a* clusters twenty-eight subbasins located in the upper basin (Figure 9a). Here, precipitation was below the basin average (1,398 mm). Figure 10a shows that the subbasins in this terminal group were considerably exposed to severe and extreme hydrological drought.

Leaves *b*, *c* and *d* cluster thirty-seven, thirteen and twenty-nine subbasins, respectively. In these subbasins, precipitation was higher than 1,398 mm. In leaf *b*, percolation was higher than 153 mm, and the curve number was higher than 51. These results suggest that the subbasins in leaf *b* experienced considerable exposure to hydrological drought (Figure 10b). Concerning leaf *d*, percolation was considerably lower than the median. Figure 10d indicates that in this terminal group, the subbasins experienced fewer months in the severe and extreme drought categories compared to leaf *a*. However, they also experienced one of the highest medians of months at moderate drought.

In leaves *e* (n = 72) and *f* (n = 18), precipitation was higher than 1,632 mm and water yield lower than 29 mm. Both terminal groups described moderate exposure to hydrological drought. Notably, at leaf *e*, the median of months in the severe and extreme drought categories was below five, while the median of months in the moderate drought category was twenty (Figure 10e). The hydrological drought exposure of the subbasins clustered at leaf *f* was also mild. In these subbasins, evapotranspiration was higher than 833 mm. These subbasins presented the lowest median of months at all drought categories. Notably, the Zapatosa marsh and upstream subbasins were clustered in this terminal group (Figure 9f).

Leaves *g* and *h* cluster seventy-one and thirty-seven subbasins, respectively. The water yield (29 mm) was considerably below the basin average at these subbasins. The MVRT indicated that surface runoff was higher than 0.5 mm. Our analysis showed that the subbasins grouped at leaf *g* presented the lowest exposure to hydrological drought. The median months at all categories were the lowest in the basin (Figure 10g). All the subbasins clustered in these leaves were upstream of the Zapatosa marsh. In leaf *h*, the surface runoff was lower than 0.5 mm. In these subbasins, the medians of months in the severe and extreme categories were relatively low, while the median of months in the moderate category was eighteen (Figure 10h).

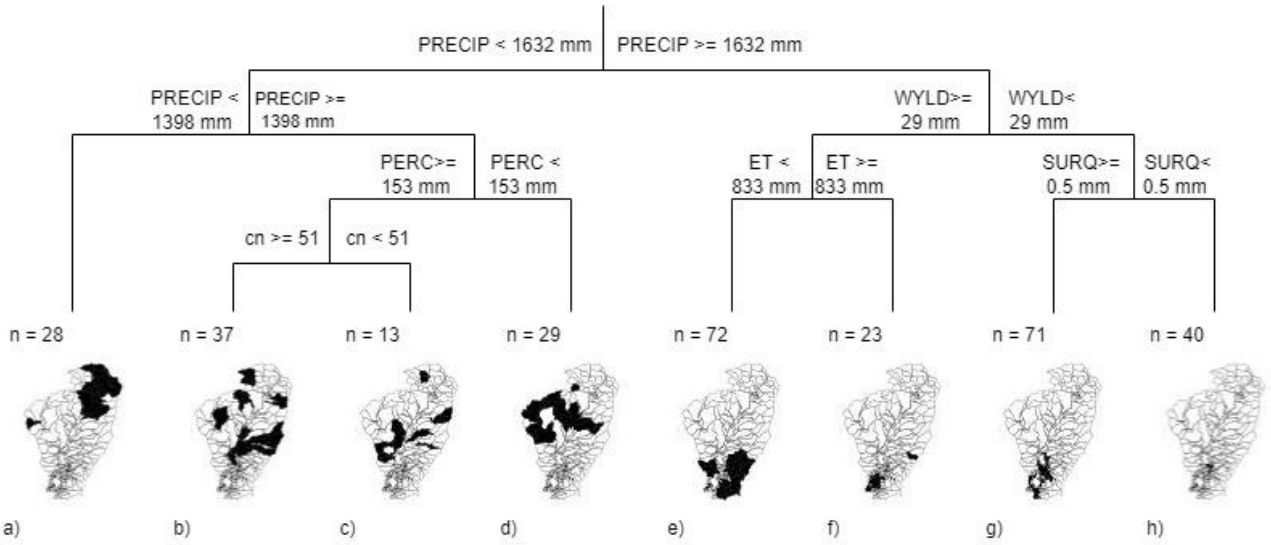

435 **Figure 9** MVRT of hydroclimatic drivers of hydrological drought at the Cesar River basin, and spatial distribution of the subbasins clustered at each leaf. Tree leaves are named from *a* to *h* and *n* indicates the number of subbasins clustered at each leaf.

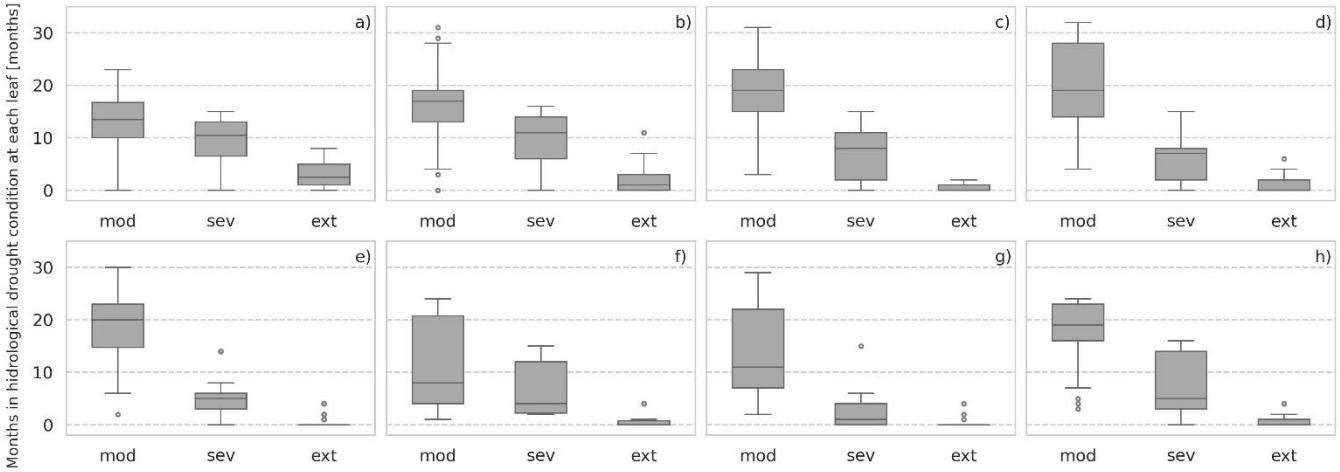

Figure 10 Months in agricultural drought categories (moderate, severe, extreme) at each leaf. Tree leaves are named from *a* to *h*.

440 **4. Discussion**

4.1 Hydroclimatic drivers of agricultural drought

The left branch of the MVRT clusters the subbasins exposed to severe agricultural drought (Figure 8a, e, f, g). Conversely, the right branch of the MVRT clusters the subbasins experiencing moderate agricultural drought severity. The subbasins in leaves *h*, *i* and *j* predominately experienced months in the moderate drought category (Figure 8i, j, k).

445

Interestingly, agricultural drought severity in leaves *a*, *e*, *f* and *g* was comparable but governed by different parameters. For instance, leaf *a* presented the highest median of months for severe and extreme agricultural drought (Figure 8a). The drought drivers in this terminal group, namely precipitation and potential evapotranspiration, indicate that agricultural drought results from an imbalance between the soil moisture supply (i.e. precipitation relatively close to the minimum value at the basin) and soil moisture demand (i.e. moderately high potential evapotranspiration). This finding aligns well with studies demonstrating that potential evapotranspiration considerably enhances the severity of agricultural droughts in water-limited areas (Ding et al., 2021; Manning et al., 2018; Teuling et al., 2013). According to such studies, potential evapotranspiration influence on agricultural drought severity may be explained by the significant increase in net radiation during droughts, as the lack of rainfall usually concurs with decreased cloud cover.

In contrast, the MVRT outcomes suggest that a lack of precipitation was not a primary driver of agricultural drought in the subbasins clustered at leaf *e*. This leaf grouped the subbasins that experienced the most severe agricultural drought in the analysis period. The median of months in the moderate drought category was above twenty; the severe category was above ten; and the extreme drought category was six (Figure 8e). The observed evapotranspiration and percolation thresholds might indicate poor precipitation partitioning and a disturbed water regime that favours water lost by runoff and evapotranspiration. Furthermore, the sediment yield threshold (notably above the median) may be linked to poor soil structure, thus compromising soil water retention capacity and enhancing drought severity.

The results from leaf *f* show that a lower sediment yield slightly reduces the severity of extreme droughts (Figure 8f), as compared to the results from leaf *e*. This is in good agreement with the findings by Masroor et al. (2022), Trnka et al. (2016) and Santra et al. (2020), who found that soil erosion enhances the characteristics of agricultural drought. Further, our results are consistent with previous studies that indicate the incidence of droughts is not only caused by extreme weather events but also by the inefficient soil–water management associated with land and soil degradation (Cornelis et al., 2019; Wildemeersch et al., 2015).

The right branch of the tree provides valuable information on the hydroclimatic parameters that reduce the severity of agricultural droughts. Moderate drought exposure levels for leaves *h*, *i* and *j* were associated with relatively low evapotranspiration thresholds; accordingly, it may be asserted that evapotranspiration controlling measures (e.g. surface cover, crop rotation, agroforestry, intercropping) are relevant interventions for building resistance to agricultural drought. At terminal groups *i* and *j*, water yield was found to influence the severity of agricultural drought. Notably, the subbasins at leaf *i* were slightly more resistant to drought (Figure 8i); this indicates that measures aimed at increasing the subbasins' water storage capacity (e.g. rainwater and floodwater harvesting techniques) are suitable interventions to reduce the severity of agricultural drought.

Some of the subbasins grouped at leaf *i* showed high exposure to hydrological drought (Figure 10b and c). Contrasting exposure to agricultural and hydrological droughts revealed that the water retention capacity in these subbasins reduced the severity of agricultural drought events but limited the contribution of surface runoff, lateral flow and groundwater to the streamflow, thus exacerbating the water deficit and hydrological drought severity. Therefore, drought management interventions require the prior assessment of the potential effects on both types of droughts.

4.2 Hydroclimatic drivers of hydrological droughts

The subbasins clustered on the left branch of the tree were the most exposed to hydrological drought (Figure 10a, b, c, d). Leaf *a* presented the highest median for months in the severe and extreme hydrological categories. The analysis results confirmed that precipitation deficits caused the severe drought (agricultural and hydrological) conditions in the upper part of the basin.

Conversely, the MVRT also showed that in terminal groups *b*, *c* and *d*, hydrological drought severity was linked to the inefficient partition of precipitation. Selected drivers (precipitation, percolation and curve number representing land use) are widely recognised as predominant drivers of hydrological droughts (Iglesias et al., 2018; Stoelzle et al., 2014; van Lanen et al., 2013; van Loon, 2015). The difference observed between the precipitation and percolation thresholds suggests that a large part of rainwater was lost either by evapotranspiration or surface runoff (or other water abstractions, e.g., human consumption, agriculture). Low percolation values limited the groundwater contribution to the streamflow, enhancing the streamflow deficit during drought periods.

Interestingly, the curve number was selected as a driver of hydrological drought for leaves *b* and *c* (Figure 9b and c). The subbasins in leaf *b* showed higher curve numbers than those in leaf *c* and higher exposure to hydrological drought. High curve number values are commonly the result of anthropogenic changes in land cover, which modifies evapotranspiration and the division of precipitation into evapotranspiration and streamflow. The present selection of the curve number at the third level of split is consistent with previous studies, which established that hydroclimatic parameters and human activities influence hydrological droughts; however, the influence of both drivers is uneven. Results indicate that hydroclimatic parameters are more influential (Jehanzaib et al., 2020; Saidi et al., 2018).

The right branch of the MVRT grouped subbasins with moderate and intermediate exposure to hydrological drought. The hydroclimatic parameters and the thresholds used to define leaves *e* and *f* (precipitation, water yield and evapotranspiration) demonstrate that in these subbasins, precipitation values compensated for the water abstraction by evapotranspiration. When we compare the severity of the hydrological droughts observed in leaves *e* and *f*, we find that lower values of evapotranspiration reduce exposure to severe and extreme hydrological drought but increase the incidence of moderate hydrological drought.

The subbasins in terminal group g experienced the lowest median number of months for all hydrological drought categories (Figure 10g). The selected drought drivers and thresholds indicate that surface runoff reaches the streamflow, and the amount of water that leaves the subbasins and contributes to the discharge downstream is limited (low water yield). Both characteristics reduced hydrological drought severity. It can be explained by the subbasins' proximity to the marsh (which acted as a natural control), the low slope in the area (which reduced streamflow velocity) and the presence of water bodies (which collected and stored runoff during the rainy season) may have enhanced the water retention capacity in these areas. The observed moderate exposure of these subbasins fits the results of earlier analyses, which found that wetlands exert significant impacts on the alleviation of hydrological drought severity when direct evaporation from the water body does not significantly reduce water storage (Wu et al., 2023). Thus, the present findings indicate that the water storage capacity of the Zapatosa marsh can compensate for the increased evaporation that occurs during drought events, thereby alleviating hydrological drought severity upstream.

The hydrological drought conditions in the subbasins clustered at leaf *h* were mild, despite water yield values below 29 mm (Figure 10h). Negligible surface runoff values indicated that in leaf *h*, rainfall is stored in the soil profile, lost by evapotranspiration or percolates in an area of minimal baseflow contribution to streamflow. This limits the amount of water reaching the streamflow and enhances the severity of hydrological droughts, compared to leaf *g*.

4.3 Comparison of the hydroclimatic parameters influencing the severity of agricultural and hydrological droughts

Crucial similarities and differences emerge from contrasting the parameters influencing the severity of droughts and the spatial distribution of the subbasins experiencing severe and mild drought conditions. MVRTs indicate that severe agricultural and hydrological drought conditions occurred in the upper and middle course of the river. Nevertheless, the severe droughts were influenced by different hydroclimatic factors. Severe agricultural drought in the headwater was driven by the interaction between precipitation shortfalls and high potential evapotranspiration (Figure 7a). Conversely, severe hydrological drought condition was solely driven by limited precipitation. It is worth highlighting that the severe hydrological situation extends from the headwater to subbasins in the middle course (Figure 9a).

Downstream, in subbasins located in the middle course, the agricultural and hydrological drought situation was also severe. In this area, droughts' severity was linked to inadequate rainfall partitioning and an unbalanced water cycle that favours water loss through evapotranspiration and low percolation values (Figure 7d, e, f and g, and Figure 9b, c and d). Significantly, agricultural and hydrological droughts in these leaves were more severe than in leaves experiencing precipitation deficits (Figure 7a and Figure 9a). Results also suggest that poor soil structure enhanced severe agricultural drought conditions (Figure 7e), and high curve numbers seem to increase hydrological drought severity (Figure 9b).

MVRTs also showed subbasins experiencing mild agricultural and hydrological drought severity. Overall, these subbasins were in the southern part of the basin. However, for agricultural drought, a few cases were observed in the north of the basin (Figure 7h, i and j). Subbasins presenting mild hydrological drought severity allocate upstream of the Zapatosa marsh (Figure 9g). Moderate agricultural drought severity was linked to low evapotranspiration losses and basin capacity to retain water in the soil profile, improving percolation (Figure 7j). In turn, moderate hydrological drought severity related to the subbasins' proximity to the marsh (which acted as a natural control reducing the water yield) and surface runoff contributions to the streamflow (Figure 9g). Remarkably, some of these subbasins also showed mild agricultural drought conditions (Figure 7i).

4.4 Accuracy of the MVRTs

The high EV (0.81) value reflects the good explanatory power of the tree built for agricultural drought. This confirms that the selected explanatory variables significantly influence the severity of agricultural drought.

Conversely, the explanatory power of the tree built for hydrological drought is not very high (EV = 0.48). This may be related to the inaccurate representation of groundwater contribution to the streamflow. Streams depend significantly on groundwater during droughts to maintain flow; nevertheless, groundwater contribution to the streamflow was not included as a key drought driver in the MVRT, although it was in the list of explanatory variables. It is possible that the model's simplifications for the simulation of groundwater flow and storage did not adequately represent the groundwater contribution to the streamflow (Molina-Navarro et al., 2019). The lack of adequate information about this relevant factor hydrological drought may have compromised the MVRT's accuracy. Unexplained variability may also link to factors that influence hydrological drought but were not considered in the dataset of explanatory variables (e.g. abstractions such as water for irrigation, industry or human consumption).

5. Conclusion

This study applied the MVRT technique, which served as an explanatory approach (in the line of 'explanatory AI') to assess the relationship between a subbasin's hydroclimatic characteristics (i.e. explanatory variables) and the severity categories of agricultural and hydrological drought (i.e. response variables). The results show that the machine learning technique successfully identifies drought severity's primary drivers and critical thresholds. The MVRT also provides valuable information on which parameters can contribute to reducing agricultural and hydrological drought severity.

Our results provide valuable information on the hydroclimatic parameters influencing the drought-generating process in the Cesar River basin. MVRTs indicate that severe agricultural and hydrological drought conditions occur in the upper and middle course of the river. Nevertheless, severe droughts are influenced by different hydroclimatic factors. The interaction between precipitation shortfalls and high potential evapotranspiration drives severe agricultural drought in the headwater. Conversely,

severe hydrological drought condition is solely caused by limited precipitation. In subbasins in the middle course, droughts' severity is linked to inadequate rainfall partitioning and an unbalanced water cycle favouring water loss through evapotranspiration and low percolation values. Notably, results suggest that poor soil structure enhances severe agricultural drought conditions, and high curve numbers seem to increase hydrological drought severity. In the southern region, subbasins experience moderate agricultural and hydrological drought severity. Mild agricultural drought is linked to low evapotranspiration losses and basin capacity to retain water in the soil profile, improving percolation. In turn, moderate hydrological drought severity relates to the subbasins' proximity to the marsh (which acted as a natural control reducing the water yield) and surface runoff contributions to the streamflow. The outcomes of this study also demonstrate that the combined effect of parameters with low impact can trigger a drought situation as severe as the one produced by one or two of the most influential parameters. It is worth mentioning that the study outcomes indicate that the slope and the soil type do not influence the severity of agricultural and hydrological droughts in the Cesar River Basin.

It can also be concluded that the MVRT (and other machine learning techniques that generate 'explainable AI' models based on progressive tree-like data partitioning and simplified models in leaves) is a relevant tool for defining drought management strategies. The tool helps researchers prioritise the areas most vulnerable to droughts and design strategies and interventions for the disturbed hydroclimatic parameters driving the droughts.

The study's limitations include its simplified approach to modelling a complex phenomenon using SWAT software (e.g. representing the groundwater components that impact hydrological drought conditions) and using only a single ML technique to build explainable models. Further extensions of this research may address these limitations. For example, candidate ML techniques could include M5 model trees (rather than regression trees), which have shown their effectiveness in solving water-related problems (see Solomatine & Dulal, 2004; Solomatine & Xue, 2004). These result in linear models in tree leaves rather than constants like in MVRT. Additionally, there is still a need to better represent anthropogenic interventions (and other relevant parameters influencing droughts) in the set of explanatory variables (e.g. abstractions such as water for irrigation, industry or human consumption, groundwater pumping).

The issue of combining human and artificial intelligence (and knowledge of physics with machine learning) is currently a point of great interest (see Jiang et al., 2020, on 'physics-aware deep learning models' and Moreido et al., 2021, on the role of experts in constraining machine-learning hydrological models). This study can be seen as one that contributes to developing and testing tools to better incorporate 'explanatory' ML techniques into existing modelling and management practices.

Data Availability. The data is available on request.

Authors contributions. All authors contributed to the study conception and design. Material preparation, data collection and analysis were performed by Ana Paez-Trujillo. Jeffer Cañon developed the hydrological model. The first draft of the manuscript was written by Ana Paez-Trujillo, and all authors commented on previous versions of the manuscript. Ana Paez-Trujillo, Jeffer Cañon, Beatriz Hernandez, Gerald Corzo and Dimitri Solomatine read and approved the final manuscript.

Competing interests. The contact author has declared that neither she nor her co-authors have any competing interest.

Acknowledgements. The authors would like to express their gratitude to the Natura Foundation and the project GEF Magdalena–Cauca VIVE for proving the hydrological model of the Cesar River basin.

Financial support. This study was financially supported by the Ministry of Education Colombia, Programa Colombia Cientifica, Grant No. 3597287. The authors have no relevant financial interest to disclose.

References

Abbaspour, K. C., Vaghefi, S. A., & Srinivasan, R. (2018). A Guideline for Successful Calibration and Uncertainty Analysis for Soil and Water Assessment: A Review of Papers from the 2016 International SWAT Conference. *Water*, *10*(6). https://doi.org/10.3390/w10010006

Arnold, J. G., Moriasi, D. N., Gassman, P. W., Abbaspour, K. C., White, M. J., Srinivasan, R., Santhi, C., Harmel, R. D., van Griensven, A., Liew, M. W. van, Kannan, N., Jha, M. K., Harmel, D., Member, A., Liew, M. W. van, & Arnold, J.-F. G. (2012). SWAT: MODEL USE, CALIBRATION, AND VALIDATION. *Transactions of the ASABE*, *55*(4), 1491–1508. http://swatmodel.tamu.edu

Borcard, D., Gillet, F., & Legendre, P. (2018). Cluster analysis. In *Numerical Ecology with R. Use R!* Springer, Cham. https://doi.org/10.1007/978-3-319-71404-2_4

Breiman, L. (2001). Random Forests. *Machine Learning*, *45*, 5–32. https://doi.org/doi.org/10.1023/A:1010933404324

Cannon, A. J. (2012). Köppen versus the computer: Comparing Köppen-Geiger and multivariate regression tree climate classifications in terms of climate homogeneity. *Hydrology and Earth System Sciences*, *16*(1), 217–229. https://doi.org/10.5194/HESS-16-217-2012

Cornelis, W., Waweru, G., & Araya, T. (2019). Building Resilience Against Drought and Floods: The Soil-Water Management Perspective. In R. Lal & R. Francaviglia (Eds.), *Sustainable Agriculture Reviews 29. Sustainable Agriculture Reviews, vol 29*. Springer, Cham. https://doi.org/https://doi.org/10.1007/978-3-030-26265-5_6

De'ath, G. (2002). MULTIVARIATE REGRESSION TREES: A NEW TECHNIQUE FOR MODELING SPECIES-ENVIRONMENT RELATIONSHIPS. *Ecology*, *83*(4), 1105–1117.

Destouni, G., & Verrot, L. (2014). Screening long-term variability and change of soil moisture in a changing climate. *Journal of Hydrology*, *516*(1), 131–139. https://doi.org/10.1016/J.JHYDROL.2014.01.059

Ding, Y., Gong, X., Xing, Z., Cai, H., Zhou, Z., Zhang, D., Sun, P., & Shi, H. (2021). Attribution of meteorological, hydrological and agricultural drought propagation in different climatic regions of China. *Agricultural Water Management*, *255*. https://doi.org/10.1016/J.AGWAT.2021.106996

GEF, BID, & Fundación Natura. (2020). *Proyecto manejo sostenible y conservacion de la biodiversidad en la cuenca del Río Magdalena. Modelo hidrológico refinado 1 en la cuenca del Río Cesar*. https://drive.google.com/file/d/1X5-iuqRPAeCjIDE-pktc0mC9cV-qKOnM/view

GEF, BID, & Fundación Natura. (2021). *Proyecto manejo sostenible y conservacion de la biodiversidad en la cuenca del Río Magdalena. Modelo hidrológico refinado 2 en la cuenca del Río Cesar*. https://drive.google.com/file/d/1sECdhG_SOYICKpjhILBtGP3fqc6y1XTk/view

Hao, Z., Hao, F., Xia, Y., Feng, S., Sun, C., Zhang, X., Fu, Y., Hao, Y., Zhang, Y., & Meng, Y. (2022). Compound droughts and hot extremes: Characteristics, drivers, changes, and impacts. *Earth-Science Reviews*, 104241. https://doi.org/10.1016/J.EARSCIREV.2022.104241

Hao, Z., & Singh, V. P. (2015). Drought characterization from a multivariate perspective: A review. *Journal of Hydrology*, *527*, 668–678. https://doi.org/10.1016/J.JHYDROL.2015.05.031

Iglesias, A., Assimacopoulos, D., & Van, L. H. A. J. (Eds.). (2018). *Drought: science and policy*. John Wiley & Sons, Incorporated. https://doi.org/10.1002/9781119017073.ch1

Instituto de hidrología, meteorología y estudios ambientales (IDEAM). (2019). *Estudio Nacional del Agua 2018*.

Jehanzaib, M., Shah, S. A., Yoo, J., & Kim, T. W. (2020). Investigating the impacts of climate change and human activities on hydrological drought using non-stationary approaches. *Journal of Hydrology*, *588 (Article 125052)*. https://doi.org/10.1016/J.JHYDROL.2020.125052

Jiang, S., Zheng, Y., & Solomatine, D. (2020). Improving AI System Awareness of Geoscience Knowledge: Symbiotic Integration of Physical Approaches and Deep Learning. *Geophysical Research Letters*, *46*, *e2020GL088229*. https://doi.org/10.1029/2020GL088229

Keyantash, J., & Dracup, J. A. (2002). *The Quantification of Drought: An Evaluation of Drought Indices*.

Konapala, G., & Mishra, A. (2020). Quantifying Climate and Catchment Control on Hydrological Drought in the Continental United States. *Water Resources Research*, *56*, e2018WR024620. https://doi.org/10.1029/2018WR024620

Kuhn, M., & Johnson, K. (2013). Over-Fitting and Model Tuning. In *Applied Predictive Modeling*. Springer, New York, NY. https://doi.org/10.1007/978-1-4614-6849-3_4

Legendre, P., & Legendre, L. (2012). Cluster analysis. In *Developments in Environmental Modelling* (Vol. 24, pp. 337–424). https://doi.org/10.1016/B978-0-444-53868-0.50008-3

Lu, J., Carbone, G. J., & Grego, J. M. (2019). Uncertainty and hotspots in 21st century projections of agricultural drought from CMIP5 models. *Sci Rep*, *9 4922*. https://doi.org/10.1038/s41598-019-41196-z

Manning, C., Widmann, M., Bevacqua, E., van Loon, A. F., Maraun, D., & Vrac, M. (2018). Soil Moisture Drought in Europe: A Compound Event of Precipitation and Potential Evapotranspiration on Multiple Time Scales. *Journal of Hydrometeorology*, *19*(8), 1255–1271. https://doi.org/10.1175/JHM-D-18-0017.1

Margariti, J., Rangecroft, S., Parry, S., Wendt, D. E., & Van Loon, A. F. (2019). Anthropogenic activities alter drought termination. *Elementa: Science of the Anthropocene 1*, *7 27*. https://doi.org/10.1525/elementa.365

Masroor, M., Sajjad, H., Rehman, S., Singh, R., Hibjur Rahaman, M., Sahana, M., Ahmed, R., & Avtar, R. (2022). Analysing the relationship between drought and soil erosion using vegetation health index and RUSLE models in Godavari middle sub-basin, India. *Geoscience Frontiers*, *13*(2), 101312. https://doi.org/10.1016/J.GSF.2021.101312

Mastrotheodoros, T., Pappas, C., Molnar, P., Burlando, P., Manoli, G., Parajka, J., Rigon, R., Szeles, B., Bottazzi, M., Hadjidoukas, P., & Fatichi, S. (2020). More green and less blue water in the Alps during warmer summers. *Nature Climate Change 2020 10:2*, *10*(2), 155–161. https://doi.org/10.1038/s41558-019-0676-5

Mckee, T. B., Doesken, N. J., & Kleist, J. (1993). The relationship of drought frequency and duration to time scales. *8th Conference on Applied Climatology, Anaheim, 17-22 January 1993*, 179–184.

Ministerio de Ambiente y Desarrollo Sostenible (Colombia). (2015). *Plan Integral de Gestión del Cambio Climático Territorial del Departamento de Cesar*.

Modarres, R. (2007). Streamflow drought time series forecasting. *Stochastic Environmental Research and Risk Assessment*, *21*(3), 223–233. https://doi.org/10.1007/S00477-006-0058-1/FIGURES/14

Molina-Navarro, E., Bailey, R. T., Andersen, H. E., Thodsen, H., Nielsen, A., Park, S., Jensen, J. S., Jensen, J. B., & Trolle, D. (2019). Comparison of abstraction scenarios simulated by SWAT and SWAT-MODFLOW. *Hydrological Sciences Journal*, *64*(4), 434–454. https://doi.org/10.1080/02626667.2019.1590583

Molnar, C. (2022). *Interpretable Machine Learning: A Guide for Making Black Box Models Explainable (2nd ed.)*. https://christophm.github.io/interpretable-ml-book/

Moreido, V., Gartsman, B., Solomatine, D. P., & Suchilina, Z. (2021). How Well Can Machine Learning Models Perform without Hydrologists? Application of Rational Feature Selection to Improve Hydrological Forecasting. *Water 2021, Vol. 13, Page 1696*, *13*(12), 1696. https://doi.org/10.3390/W13121696

Moriasi, D. N., Arnold, J. G., Van Liew, M. W., Bingner, R. L., Harmel, R. D., & Veith, T. L. (2007). Model evaluation guidelines for systematic quantification of accuracy in watershed simulations. *Transactions of the ASABE*, *50*(3), 885–900.

Narasimhan, B., & Srinivasan, R. (2005). Development and evaluation of Soil Moisture Deficit Index (SMDI) and Evapotranspiration Deficit Index (ETDI) for agricultural drought monitoring. *Agricultural and Forest Meteorology*, *133*(1–4), 69–88. https://doi.org/10.1016/j.agrformet.2005.07.012

Peña-Gallardo, M., Vicente-Serrano, S. M., Hannaford, J., Lorenzo-Lacruz, J., Svoboda, M., Domínguez-Castro, F., Maneta, M., Tomas-Burguera, M., & Kenawy, A. el. (2019). Complex influences of meteorological drought time-scales on hydrological droughts in natural basins of the contiguous Unites States. *Journal of Hydrology*, *568*, 611–625. https://doi.org/10.1016/J.JHYDROL.2018.11.026

Prudhomme, C., Giuntoli, I., Robinson, E. L., Clark, D. B., Arnell, N. W., Dankers, R., Fekete, B. M., Franssen, W., Gerten, D., Gosling, S. N., Hagemann, S., Hannah, D. M., Kim, H., Masaki, Y., Satoh, Y., Stacke, T., Wada, Y., & Wisser, D. (2014). Hydrological droughts in the 21st century, hotspots and uncertainties from a global multimodel ensemble experiment. *Proceedings of the National Academy of Sciences of the United States of America*, *111*(9), 3262–3267. https://doi.org/10.1073/PNAS.1222473110/SUPPL_FILE/PNAS.201222473SI.PDF

Rangecroft, S., Van Loon, A. F., Maureira, H., Verbist, K., & Hannah, D. M. (2019). An observation-based method to quantify the human influence on hydrological drought: upstream–downstream comparison. *Hydrological Sciences Journal*, *64*(3), 276–287. https://doi.org/10.1080/02626667.2019.1581365

Saft, M., Peel, M. C., Western, A. W., & Zhang, L. (2016). Predicting shifts in rainfall-runoff partitioning during multiyear drought: Roles of dry period and catchment characteristics. *Water Resources Research*, *52*(12), 9290–9305. https://doi.org/10.1002/2016WR019525

Saidi, H., Dresti, C., Manca, D., & Ciampittiello, M. (2018). Quantifying impacts of climate variability and human activities on the streamflow of an Alpine river. *Environmental Earth Sciences*, *77*(19), 1–16. https://doi.org/10.1007/S12665-018-7870-Z/TABLES/5

Santra, A., & Santra Mitra, S. (2020). Space-Time Drought Dynamics and Soil Erosion in Puruliya District of West Bengal, India: A Conceptual Design. *Journal of the Indian Society of Remote Sensing*, *48*(8), 1191–1205. https://doi.org/10.1007/S12524-020-01147-Y/TABLES/5

Seneviratne, S. I., Nicholls, N., Easterling, D., Goodess, C. M., Kanae, S., Kossin, Y., Luo, Y., Marengo, J., McInnes, K., Rahimi, M., Reichstein, M., Sorteberg, A., Vera, C., & Zhang, X. (2012). Changes in Climate Extremes and their Impacts on the Natural Physical Environment. In C. B. Field, V. Barros, T. F. Stocker, D. Qin, D. J. Dokken, K. L. Ebi, M. D. Mastrandrea, Mach K.J., G.-K. Plattner, S. K. Allen, M. Tignor, & Midgley P.M (Eds.), *Managing the Risks of Extreme Events and Disasters to Advance Climate Change Adaptation* (pp. 109–230). Cambridge University Press, UK, and New York, NY, USA.

Shah, D., Shah, H. L., Dave, H. M., & Mishra, V. (2021). Contrasting influence of human activities on agricultural and hydrological droughts in India. *Science of the Total Environment*, *774*. https://doi.org/10.1016/J.SCITOTENV.2021.144959

Sheffield, J., & Wood, E. F. (2011a). The science of drought. In *Drought: Past Problems and Future Scenarios* (pp. 18–42). Taylor & Francis Group.

Sheffield, J., & Wood, E. F. (2011b). What is drought. In *Drought: Past Problems and Future Scenarios* (pp. 9–15). Taylor & Francis Group.

Solomatine, D. P., & Xue, Y. (2004). M5 Model Trees and Neural Networks: Application to Flood Forecasting in the Upper Reach of the Huai River in China. *Journal of Hydrologic Engineering*, *9*(6), 491–501. https://doi.org/10.1061/(asce)1084-0699(2004)9:6(491)

Stoelzle, M., Stahl, K., Morhard, A., & Weiler, M. (2014). Streamflow sensitivity to drought scenarios in catchments with different geology. *Geophysical Research Letters*, *41*(17), 6174–6183. https://doi.org/10.1002/2014GL061344

Teuling, A. J., van Loon, A. F., Seneviratne, S. I., Lehner, I., Aubinet, M., Heinesch, B., Bernhofer, C., Grünwald, T., Prasse, H., & Spank, U. (2013). Evapotranspiration amplifies European summer drought. *Geophysical Research Letters*, *40*(10), 2071–2075. https://doi.org/10.1002/GRL.50495

The World Bank. (2021). *Groundswell Part 2: Acting on Internal Climate Migration*. www.worldbank.org

Tijdeman, E., Barker, L. J., Svoboda, M. D., & Stahl, K. (2018). Natural and Human Influences on the Link Between Meteorological and Hydrological Drought Indices for a Large Set of Catchments in the Contiguous United States. *Water Resources Research*, *54*(9), 6005–6023. https://doi.org/10.1029/2017WR022412

Transactions of the ASABE (American Society of Agricultural and Biological Engineers). (2018). *Guidelines for Calibrating, Validating, and Evaluating Hydrologic and Water Quality (H/WQ) Models*. *61(4): 1393-1401*. https://doi.org/doi: 10.13031/trans.12806

Trnka, M., Semerádová, D., Novotný, I., Dumbrovský, M., Drbal, K., Pavlík, F., Vopravil, J., Štěpánková, P., Vizina, A., Balek, J., Hlavinka, P., Bartošová, L., & Žalud, Z. (2016). Assessing the combined hazards of drought, soil erosion and local flooding on agricultural land: A Czech case study. *Climate Research*, *70*(2–3), 231–249. https://doi.org/10.3354/cr01421

Universidad del Atlantico. (2014). *Plan de ordenamiento del recurso hidrico del Rio Cesar Formulacion Final*.

Universidad del Magdalena, CORPAMAG, & CORPOCESAR. (2017). *Documento sintesis para la declaratoria del complejo cenagso de la Zapatosa como area protegida*.

USDA. (2007). Hydrologic Soil Groups. In *Hydrology National Engineering Handbook*.

Valiya Veettil, A., & Mishra, A. k. (2020). Multiscale hydrological drought analysis: Role of climate, catchment and morphological variables and associated thresholds. *Journal of Hydrology*, *582*, 124533. https://doi.org/10.1016/J.JHYDROL.2019.124533

Van Lanen, H. A. J., Wanders, N., Tallaksen, L. M., & Van Loon, A. F. (2013). Hydrological drought across the world: Impact of climate and physical catchment structure. *Hydrology and Earth System Sciences*, *17*(5), 1715–1732. https://doi.org/10.5194/HESS-17-1715-2013

Van Loon, A. F. (2015). Hydrological drought explained. *Wiley Interdisciplinary Reviews: Water*, *2*(4), 359–392. https://doi.org/10.1002/WAT2.1085

Van Loon, A. F., Huijgevoort, M. H. J. Van, & Van Lanen, H. A. J. (2012). Evaluation of drought propagation in an ensemble mean of large-scale hydrological models. *Hydrol. Earth Syst. Sci*, *16*, 4057–4078. https://doi.org/10.5194/hess-16-4057-2012

Vicente-Serrano, S. M., López-Moreno, J. I., Beguería, S., Lorenzo-Lacruz, J., Azorin-Molina, C., & Morán-Tejeda, E. (2011). Accurate Computation of a Streamflow Drought Index. *Journal of Hydrologic Engineering*, *17*(2), 318–332. https://doi.org/10.1061/(ASCE)HE.1943-5584.0000433

Vicente-Serrano, S. M., Quiring, S. M., Peña-Gallardo, M., Yuan, S., & Domínguez-Castro, F. (2020). A review of environmental droughts: Increased risk under global warming? *Earth-Science Reviews*, *201*. https://doi.org/10.1016/J.EARSCIREV.2019.102953

Wang, M., Jiang, S., Ren, L., Xu, C. Y., Menzel, L., Yuan, F., Xu, Q., Liu, Y., & Yang, X. (2021). Separating the effects of climate change and human activities on drought propagation via a natural and human-impacted catchment comparison method. *Journal of Hydrology*, *603*. https://doi.org/10.1016/J.JHYDROL.2021.126913

Wildemeersch, J. C. J., Garba, M., Sabiou, M., Fatondji, D., & Cornelis, W. M. (2015). Agricultural drought trends and mitigation in Tillaberí, Niger. *Soil Science and Plant Nutrition*, *61*(3), 414–425. https://doi.org/10.1080/00380768.2014.999642

WMO, & GWP. (2016). *Handbook of Drought Indicators and Indices (M. Svoboda and B.A. Fuchs)*. Integrated Drought Management Programme (IDMP), Integrated Drought Management Tools and Guidelines Series 2.

Wu, Y., Sun, J., Blanchette, M., Rousseau, A. N., Xu, Y. J., Hu, B., & Zhang, G. (2023). Wetland mitigation functions on hydrological droughts: From drought characteristics to propagation of meteorological droughts to hydrological droughts. *Journal of Hydrology*, *617*, 128971. https://doi.org/10.1016/J.JHYDROL.2022.128971

Xu, Y., Zhang, X., Wang, X., Hao, Z., Singh, V. P., & Hao, F. (2019). Propagation from meteorological drought to hydrological drought under the impact of human activities: A case study in northern China. *Journal of Hydrology*, *579*, 124147. https://doi.org/10.1016/J.JHYDROL.2019.124147

Zargar, A., Sadiq, R., Naser, B., & Khan, F. I. (2011). A review of drought indices. *Reviews*, *19*, 333–349. https://doi.org/10.2307/envirevi.19.333

Zhang, X., Hao, Z., Singh, V. P., Zhang, Y., Feng, S., Xu, Y., & Hao, F. (2022). Drought propagation under global warming: Characteristics, approaches, processes, and controlling factors. *Science of The Total Environment*, *838*, 156021. https://doi.org/10.1016/J.SCITOTENV.2022.156021